Composites: Part A 59 (2014) 30–36

Contents lists available at ScienceDirect

Composites: Part A

journal homepage: www.elsevier.com/locate/compositesa

Evolution of lignocellulosic fibre lengths along the screw profile during twin screw compounding with polycaprolactone

Françoise Berzin [a,b,*], Bruno Vergnes [c], Johnny Beaugrand [a,b]

[a] Université de Reims Champagne-Ardenne, UMR614 Fractionnement des AgroRessources et Environnement, F-51100 Reims, France
[b] INRA, UMR614 Fractionnement des AgroRessources et Environnement, F-51686 Reims, France
[c] MINES ParisTech, Centre de Mise en Forme des Matériaux (CEMEF), CS 10207, F-06904 Sophia Antipolis, France

ARTICLE INFO

Article history:
Received 10 June 2013
Received in revised form 3 December 2013
Accepted 14 December 2013
Available online 28 December 2013

Keywords:
A. Fibres
B. Fragmentation
C. Computational modelling
E. Extrusion

ABSTRACT

Composites made of polycaprolactone reinforced by 20% hemp fibres were prepared by melt blending in a twin screw extruder (TSE). The influence of the extrusion parameters (feed rate and screw speed) on the fibre length evolution along the screw profile was investigated. The fibre length rapidly decreased after the introduction of the fibres and during the flow through the kneading blocks. Fibre fragmentation was increased at high screw speeds and low feed rates. The flow conditions along the TSE were calculated using Ludovic© software, focusing on the specific mechanical energy (SME) provided to the fibres. The fibre length evolution can be correctly estimated for various flow conditions using an exponential function of the SME.

1. Introduction

The use of lignocellulosic fibres to reinforce polymers and to design composite materials is growing due to bioeconomy requirements, the sustainability of this natural resource, its relatively low cost and its weight advantage when compared to glass or carbon fibres [1–3]. Natural fibres composites are usually produced by compounding fibres with other materials in twin screw extruders. As for synthetic fibres, the main problem is the change in fibre length (L) and aspect ratio (L/D, length/diameter), due to the high stresses encountered during the process. Individual fibres are generally cemented together into bundles, and then into a group of bundles, by a matrix that consists of several amorphous polymers [4,5]. The defibrization process concomitantly results in decohesion (when a fracture occurs in the interfibre cement) and in fragmentation of the fibre elements. Fragmentation occurs when the intrafibre cell wall is damaged, which is comparable to the breakage that occurs in synthetic fibres (i.e., glass fibre). During the extrusion process, both decohesion and fragmentation occur in the composite material, leading to fibre individualization and length reduction [6–8]. Contrary to rigid glass fibres, whose rupture mechanisms are well known and modelled [9–12], lignocellulosic fibres are generally flexible and can entangle to form large aggregates. Novel insights about flax fibre ruptures were recently provided through direct observations using rheo-optics [13]. Rupture by fatigue was observed, and the authors confirmed that natural defects (“kink bands”) initially present on flax fibres strongly affect the rupture location. The influence of thermomechanical conditions on the fibre cell wall properties [14] and on the fibre length and aspect ratio have been studied with internal mixers [15] or TSEs [16–20]. In a previous study [20], we demonstrated that differences in defibrization affect the fibre L/D ratio, which in turn influences the mechanical properties of the final composite. This phenomenon was also observed by Jiang et al. [21]. Regarding the process parameters, the final fibre length was reduced with decreasing feed rates and increasing screw speeds. In contrast, the L/D ratio was less affected by changes in the above-mentioned processing conditions, indicating a simultaneous reduction in fibre length and diameter. The fibre length and aspect ratio could be roughly evaluated for different processing conditions using an exponential function of the specific mechanical energy, as suggested for glass fibres by Inceoglu et al. [10].

In this paper, we describe the development of a predictive lignocellulosic defibrization model by following the length evolution along the screws during TSE compounding. This work involved the same polycaprolactone matrix, lignocellulosic fibre (hemp) and TSE materials as described in a previous study [20]. We characterized the evolution of the fibre length distribution along the screw profile for different processing conditions and established a theoretical model describing these results.

* Corresponding author at: Université de Reims Champagne-Ardenne, UMR614 Fractionnement des AgroRessources et Environnement, F-51100 Reims, France.
E-mail address: francoise.berzin@univ-reims.fr (F. Berzin).

1359-835X/$ - see front matter © 2013 Elsevier Ltd. All rights reserved.
http://dx.doi.org/10.1016/j.compositesa.2013.12.008

2. Experimental

2.1. Materials

The matrix consists of polycaprolactone (PCL), selected for its low melting temperature (60 °C), which is of interest when compounding lignocellulosic fibres. PCL (Capa© 6800), provided by Perstorp (United Kingdom), has a molecular weight of 80,000 g/mol and a melt flow index (MFI) of 3 g/10 min (160 °C, 2.16 kg). At 160 °C, PCL is quasi-Newtonian with a viscosity of 230 Pa s, as shown in Fig. 1.

The fibres used in this study originate from hemp stems (*Cannabis sativa L*, variety: Fedora 17) grown in Aube (France) in 2009 and were supplied by Fibres Recherche Développement® (Troyes, France). To minimize the heterogeneity and the length dispersion, kilograms of long scutched bast fibres were manually hacked and chopped into a homogeneous masterbatch approximately 1.4 ± 0.34 cm in length. Initial average diameter of the hemp fibres was around 300 μm, leading to a L/D ratio of 47. The fibre samples were preconditioned at 50% relative humidity in a climatic chamber before testing.

2.2. Extrusion conditions

The composites were prepared using a laboratory-scale TSE Clextral BC 21 (Firminy, France). The extruder has a diameter (D) of 25 mm and a length (L) of 900 mm (L/D ratio: 36). The screw profile used is shown in Fig. 2. The TSE is composed of a block of kneading discs with staggering angles of −45° for melting, followed by a second one with angles of 90° and then by a third with angles of −45° (Table 1). PCL and hemp fibres can be introduced either simultaneously in the hopper (barrel 1, before the melting zone) or in two steps (PCL in barrel 1 and all the fibres in barrel 4, after PCL melting). In all cases, a venting zone for eventual water steam evacuation is located in barrel 7.

The barrel temperature was set at 100 °C, and the experiments consisted of varying the flow rate (1, 2 and 3 kg/h) at a constant screw speed (200 rpm) and varying the screw speed (100, 150, 200 and 300 rpm) at a constant flow rate (2 kg/h), as described in Table 2. The fibres were mixed with PCL at a concentration of 20 wt.%. The fibres were fed manually to prevent possible irregular feeding, which usually occurs with long fibres when using either volumetric or gravimetric feeders. Before the experiment, a lot of beakers were prepared, with 2 g of fibres in each of them. During the extrusion, they were poured each 15 seconds into the feeder or the barrel opening. It was checked that this methodology ensured a very stable and constant feeding. After reaching steady-state conditions, the feeding and screw rotation were suddenly stopped, the barrel was cooled by water circulation and the barrel was extracted. The samples were then obtained from the screws at different locations, as indicated in Fig. 2 (positions 1–6: fibres are introduced before the melting zone; positions 4–6: fibres are introduced after the melting zone).

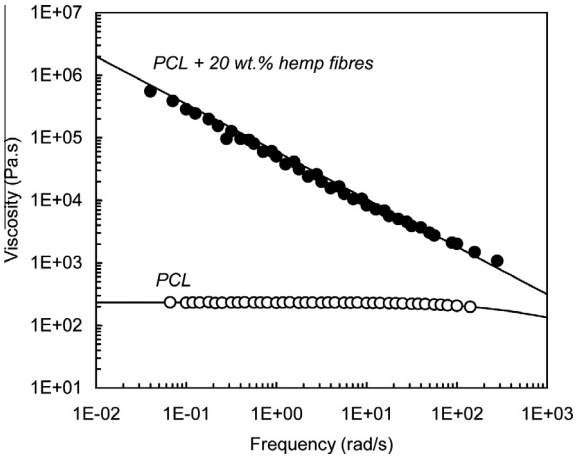

Fig. 1. Viscosity curves of PCL and composite with 20 wt.% fibres at 160 °C. Symbols are experimental points, full lines are fits by a Carreau–Yasuda law (PCL) or a power law (PCL + 20 wt.% hemp fibres).

2.3. Flow modelling

To estimate the parameter values that cannot be measured experimentally during the compounding process, we used Ludovic© flow simulation software dedicated to TSE [22]. Specifically, Ludovic© was used to calculate the specific mechanical energy (SME) transmitted to the composite all along the extruder and to predict the average length evolution during the compounding process.

2.4. Composite characterization

After extrusion, the samples were analyzed to quantify the fibre length distribution. First, the PCL matrix was extracted using the Soxhlet methodology [20] to determine the fibre content. This technique was employed to evaluate the possible fibre content variation during compounding and to verify that the average value satisfied the 20% target.

The fibre dimensions and morphologies were further obtained via image analyses using optical microscopy and MorFi software (Techpap, Grenoble, France). A mass of approximately 0.6 g was diluted in water extemporarily, and the fibres were tested in duplicate or triplicate samples to determine their mean values. Over 100,000 elements were counted for each sample. By convention, elements having a length of >200 μm were considered fibres, while shorter elements were considered fines. This limit is imposed by the MorFi system. It corresponds roughly to the length under which the mechanical reinforcement is less interesting. The fibre elements were further characterized by their aspect ratio L/D. However, elements longer than approximately 10 mm cannot be analyzed with this system due to technical restrictions. Fortunately, these long fibres remained seldom in the extruded samples. Moreover, although optimized dilution procedures were used, when agglomerates of entangled long fibres were present, they could not be taken into account via the employed method. In this case, the calculated distribution was underestimated, and the values were not used in the discussion.

3. Results and discussion

3.1. Extrusion conditions

First, focusing on the extrusion conditions that define the thermomechanical treatment received by the hemp fibres during the compounding process is necessary. Indeed, a temperature of >160 °C has been reported to affect fibre properties [20], and the conditions (e.g., inert atmosphere, presence of oxygen, temperature ramp and time of exposition) can modify the thermal degradation temperature [23]. Moreover, we previously demonstrated the relationships between the SME and fibre dimensions [20]. Fig. 3 shows the final product temperature variations, measured at the die exit, and the global specific energy, deduced from the extruder torque, as functions of the screw speed. With these results, we observed a linear increase in both parameters with increasing screw speed. The maximum temperature is 158 °C, which should prevent

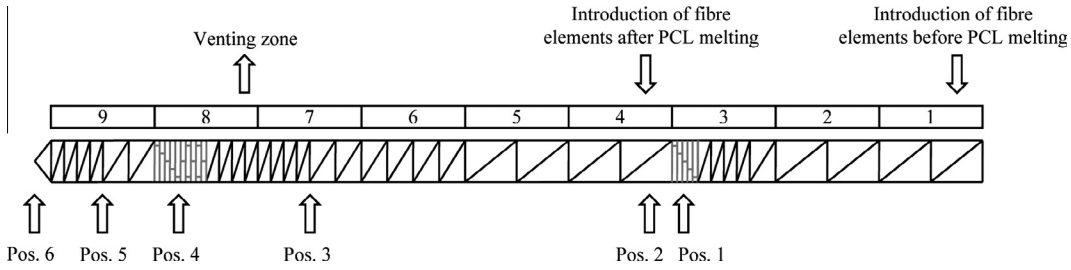

Fig. 2. Screw profile used in the experiments and sampling locations.

Table 1
Screw profile (from hopper to die).

Length (mm)	200	25	25	25	150	200	100	25	25	50	50
Pitch (mm)	33	25	16	KB[a] −45/5	33	25	16	KB[a] 90/5	KB[a] −45/5	25	16

[a] KB −45/5 indicates the kneading disc blocks of 5 elements with a staggering angle of −45° (left-handed).

Table 2
Process parameters for extrusion (Clextral BC 21).

Screw speed (rpm)	Introduction of fibres	Total feed rate (kg/h)	Sample locations
200 rpm	Before melting	1	1, 2, 3, 4, 5, 6
	After melting	1	4, 5, 6
	Before melting	2	1, 2, 3, 4, 5, 6
	After melting	2	4, 5, 6
	Before melting	3	1, 2, 3, 4, 5, 6
	After melting	3	4, 5, 6
Total feed rate (kg/h)	**Introduction of fibres**	**Screw speed (rpm)**	**Sample locations**
2 kg/h	After melting	100	4, 5, 6
		150	4, 5, 6
		200	4, 5, 6
		300	4, 5, 6

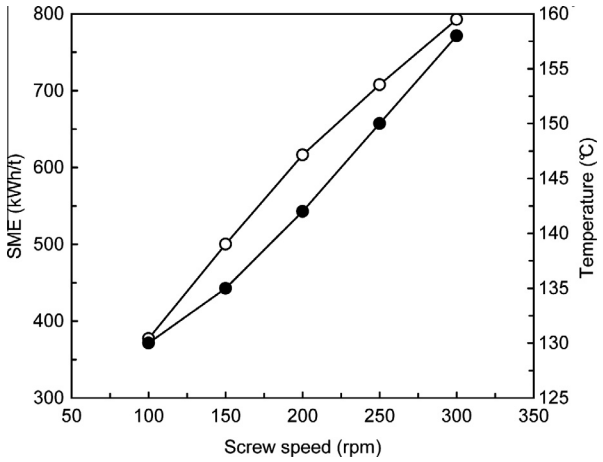

Fig. 3. Change in the global SME (○) and the exit temperature (●) with screw speed when fibres are introduced in barrel 4.

fibre thermal degradation. When the feed rate is varied between 1 and 3 kg/h, the SME decreases, but the temperature is less affected. When the fibres are introduced in barrel 1 instead of 4, the final temperature and the SME are slightly higher, by 2–4 °C and by 30–50 kW h/t, respectively (data not shown in Fig. 3).

To determine the evolution of the process parameters along the screws, we used the modelling software Ludovic© [22]. Viscosity values for PCL and the composites with 20% fibres, which are required for the calculation performed in the software, were previously determined [20] and are shown in Fig. 1. As an example, we show in Fig. 4 the evolution along the screw profile of the global SME (that we can compare to experimental values) and of the SME provided to the product after the introduction of fibres in barrel 4. We observed that the SME increases primarily in the blocks of the kneading discs and in the filled section prior to the die. In the presented case (1 kg/h, 200 rpm), when the fibres are introduced in barrel 4, the SME provided to the composite is approximately 76% of the global SME.

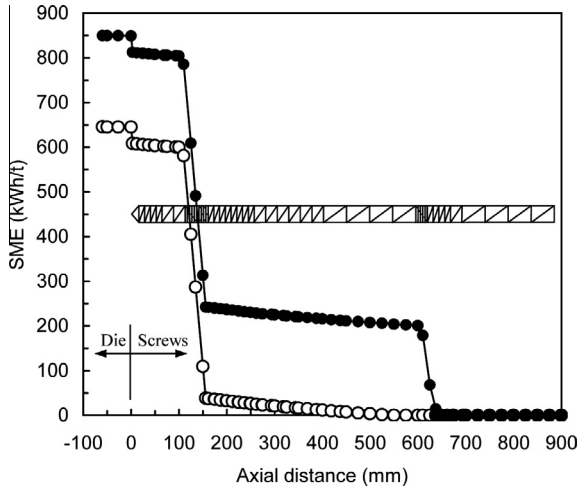

Fig. 4. Evolution along the screws of the global SME (●) and the SME provided after the introduction of fibres in barrel 4 (○) (1 kg/h, 200 rpm).

To validate the simulation, we present a comparison between the calculated and the measured global SME values for the various conditions tested in Fig. 5 (i.e., varying the screw speed and the feed rate). Thus, even though the model tends to underestimate the data by approximately 15%, the agreement is rather good over the entire range of the SME (i.e., between 300 and 1100 kW h/t).

3.2. Fibre dimensions

3.2.1. General results

Quantifying fibre dimensions is a difficult task, which can obviously be influenced by the method used [24,25]. As in our previous study [20], we employed the MorFi© system, due to the preferred statistical significance (>100,000 elements analyzed) and the "automatic technique" aspect, rather than a "laboratory made" measurement. However, as previously described, some long fibres (approximately $\geqslant$10 mm) cannot be analyzed with this system, and thus the results must carefully be considered.

Fig. 6 shows a general example of the fibre element length distributions obtained at the die exit at 1 kg/h and 200 rpm when fibres were introduced in barrel 4. First, note that the majority (97%) of the measured elements are constituted by fines, i.e., fragments arbitrarily defined by a dimension of <200 μm (576,811 fines and 15,192 fibres were measured in this case). Independent of the processing conditions and sample locations, the average lengths of the fines fall in the range of 19–38 μm. Because these fines are very short, their influence on composite reinforcement is still under question. Therefore, in the following section, we will focus on the known reinforcement elements, i.e., the fibres defined by a length >200 μm. As shown in Fig. 6, when compared to the initial fibre elements (L = 14 mm), the lengths of the extruded fibres were drastically reduced, with a final average value of 383 μm (>36-fold reduction). The maximum fibre length was approximately 5 mm (we recall that the eventual remaining fibres longer than 10 mm cannot be considered). In addition to length reduction, the average fibre width was also reduced, from 300 μm for the initial fibres to 20 μm, indicating the occurrence of bundle decohesion during compounding, as expected. As a consequence, the fibre aspect ratio was also reduced, from 46 to 19. Similar distributions were obtained for the other processing conditions and locations along the screws.

3.2.2. Influence of the processing conditions

The evolution of the average fibre lengths along the screws is shown in Fig. 7 for the two flow rates used when introducing the fibres in barrel 1. We observed a very strong reduction after the solid conveying and the melting process, where the average length was approximately 1 mm (14 mm initial fibres). However, the longer fibres may have aggregated into bundles and were not accounted for in the characterization. Nevertheless, the length reduction continues in the following processing steps, more specifically in the region of the kneading blocks. The evolution of the fibre lengths is similar for both flow rates, and the average length decreases when the feed rate is decreased, most likely due to the increased residence time.

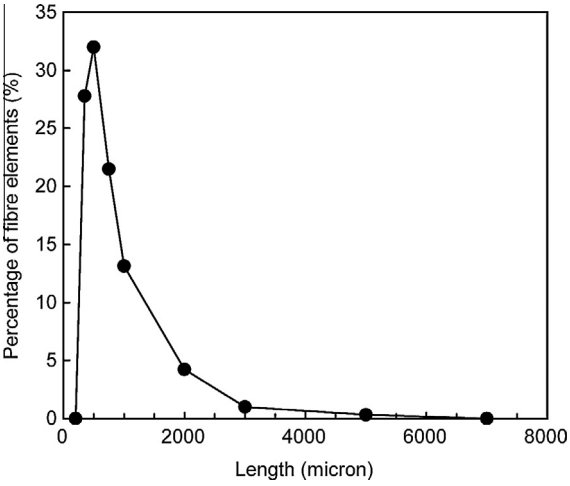

Fig. 6. Fibre length distribution at the die exit (1 kg/h, 200 rpm, fibre introduction after melting).

When the fibres are introduced in barrel 4, after the melting stage, the characterization is more difficult; reliable data were only obtained for the three last points due to the technical problems discussed in the previous section. However, the results indicate that the fibres are more preserved (Fig. 8). The influence of the screw speed is shown in Fig. 9. In all cases, we observed a significant length reduction during the flow through the kneading block and in the final part of the screws. As expected, the fibre lengths decrease when the screw speed increases due to the increased shear rate.

In all cases, the fibre width is more or less similar, approximately 20 μm, indicating that bundle decohesion most likely occurs in the first moments after fibre introduction. Consequently, along the screws, the L/D ratio follows the same evolution as the

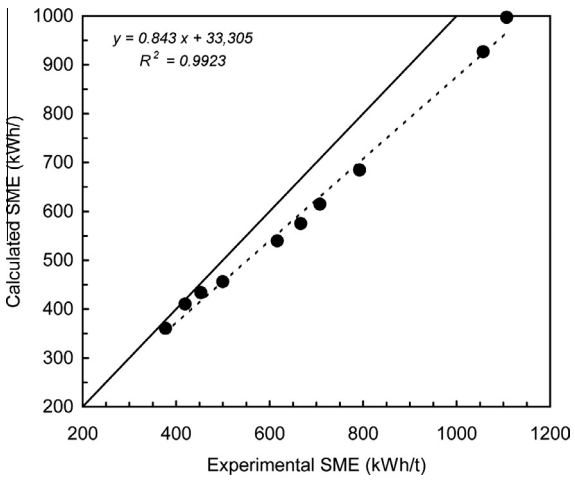

Fig. 5. Comparison of the calculated and measured SME values.

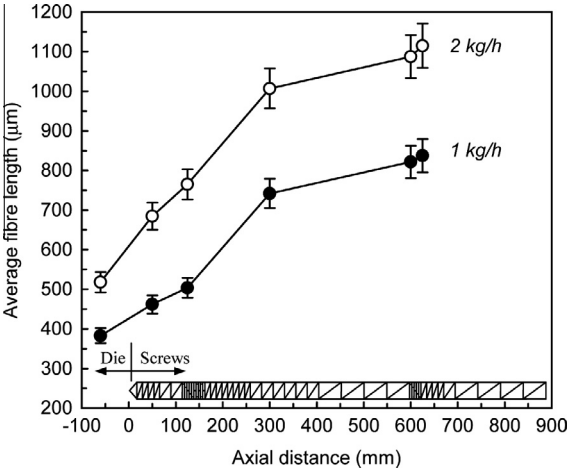

Fig. 7. Influence of the feed rate on the evolution of the average measured fibre length along the screws (200 rpm, fibre introduction before melting).

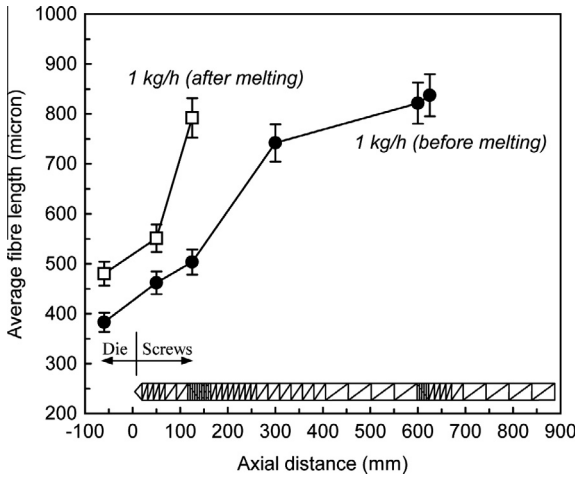

Fig. 8. Influence of fibre introduction on the evolution of average fibre length along the screws (200 rpm, 1 kg/h).

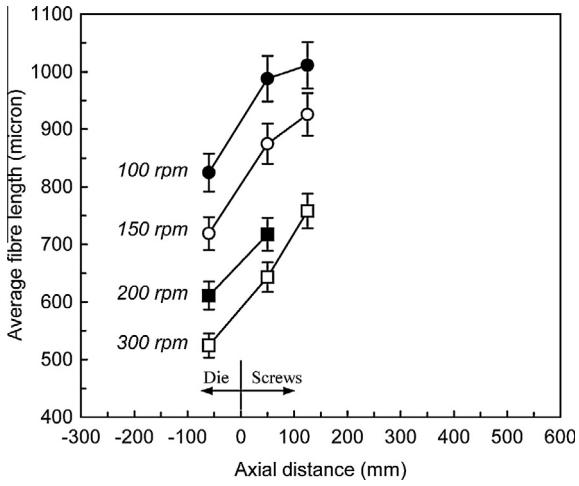

Fig. 9. Influence of the screw speed (● 100 rpm, ○ 150 rpm, ■ 200 rpm, □ 300 rpm) on the evolution of the average fibre length along the screws (1 kg/h, fibre introduction in barrel 4, after melting).

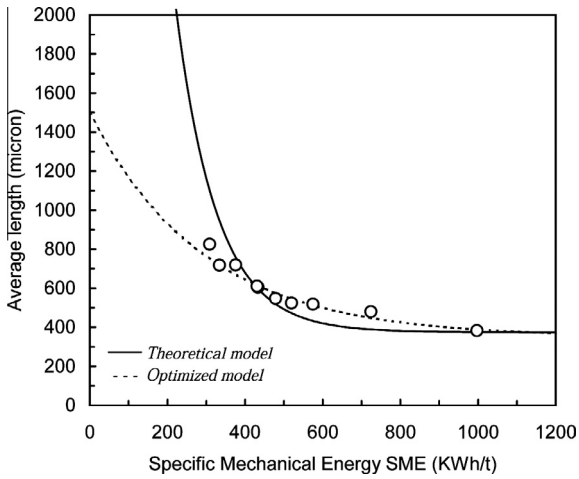

Fig. 10. Evolution of the average fibre length along the screws as a function of the SME. A comparison of the experiments (symbols) and the model (full line: previous values, dotted line: optimized values) (200 rpm, 1 kg/h, fibre introduction before melting) is shown.

average length. These results differ from what was observed at the die exit in a previous study [20] where the L/D ratio was found less affected by the processing conditions.

3.2.3. Modelling of fibre length evolution

Inceoglu et al. [10] demonstrated that the glass fibre length after compounding could be related to the SME through a relationship derived from the initial work of Shon et al. [26]. However, this relationship could not be used to follow the length evolution along the screws, for which a mechanistic model based on the true break up mechanism must be used [11,12]. In our previous work [20], we showed that a relationship between the fibre length and the SME could also be applied to hemp fibres. For various processing conditions and screw profiles, the final average fibre length, L, can be expressed as:

$$L = L_\infty + (L_0 - L_\infty)\exp(-K\ SME), \tag{1}$$

where L_0 is the initial value, L_∞ represents the limit value, K is a constant and SME represents the specific mechanical energy after the introduction of the fibres. In our case, we used the following values: L_0 = 14,000 μm, L_∞ = 350 μm and K = 0.009 (kW h/t)$^{-1}$. Fig. 10

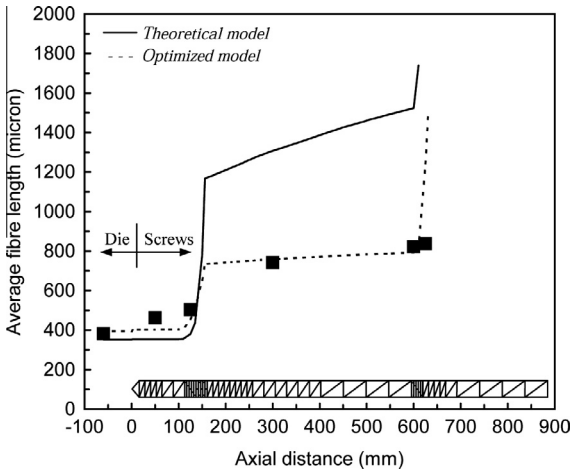

Fig. 11. Evolution of the average fibre length along the screws. A comparison of the model (full and dotted lines) and the experiments (symbols) (200 rpm, 1 kg/h, fibre introduction before melting) is shown.

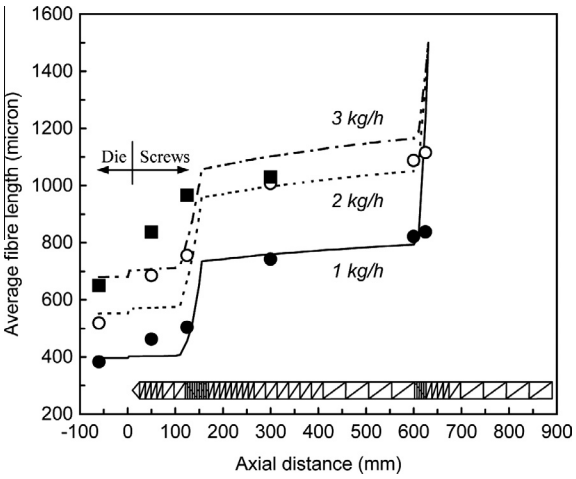

Fig. 12. Influence of the feed rate on the evolution of the average fibre length along the screws. A comparison between the experiments (symbols) and the model (full line) (200 rpm, ● 1 kg/h, ○ 2 kg/h, ■ 3 kg/h, fibre introduction before melting) is shown.

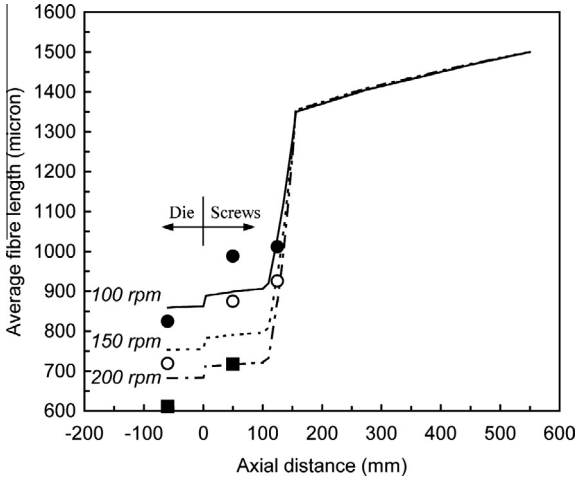

Fig. 13. Influence of the screw speed on the evolution of the average fibre length along the screws. A comparison between the experiments (symbols) and the model (full line) (2 kg/h, ● 100 rpm, ○ 150 rpm, ■ 200 rpm, fibre introduction after melting) is shown.

indicates that this law describes the correct trend, but it does not exactly fit the experimental data. A much better fit can be obtained after changing the parameters to the following: $L_0 = 1500$ μm, $L_\infty = 350$ μm and $K = 0.0035$ (kW h/t)$^{-1}$; afterwards, the agreement is improved.

Because we can calculate the evolution of the SME along the screws (Fig. 4), we can use Eq. (1) to predict the corresponding change in fibre length, at least after the melting zone, because the SME is not calculated during the solid conveying and melting. With the previous values, we obtained the results presented in Fig. 11. Although the general trends are correct, the model largely overestimates the fibre lengths along the main part of the screw profile. However, with the new values, the theoretical model fits the fibre length evolution well. Moreover, Fig. 12 indicates that the effect of varying the feed rate is correctly predicted (Note: the two first points are missing at 3 kg/h, where unrealistic results were obtained due to the presence of fibres >10 mm obstructing the MorFi analyzer).

The effect of screw speed is shown in Fig. 13 (fibre introduction in barrel 4). Once again, the global trends are correctly predicted using the optimized model, with decreases in fibre lengths when the screw speed is increased. Thus, with the appropriate parameters, Eq. (1) is able to describe the changes in average fibre lengths along the screw profile for the various processing conditions, which is not the case for rigid glass fibres [11,12]. For long flexible fibres, a criterion based on energy appears more appropriate. However, the choice of the initial fibre length ($L_0 = 1500$ μm) is crucial, which indicates that this model can only be applied once the fibres have been reduced to a certain length. The first decohesion and fragmentation mechanisms of 14 mm long pristine fibres likely obey different kinetics and cannot be considered by this simplified model.

4. Conclusions

We have prepared composites made of PCL and hemp fibres by twin screw extrusion under various processing conditions. We collected fibre samples along the screw profile and characterized their dimensions. The fibres are subjected to severe defibrization (decohesion and fragmentation) during the extrusion process, specifically at high screw speeds and low feed rates. We calculated the specific mechanical energy evolution along the screw profile and predicted fibre length changes according to an exponential function. The general predictions of the model are in agreement with the measurements, but indicate that the initial defibrization process requires further study. Complementary experiments are also necessary to verify if the presented model could be generalized to other lignocellulosic typologies, such as wood or other annual plant long fibres.

Acknowledgments

The authors thank FRD (Troyes, France) for providing hemp fibres, the Région Champagne-Ardenne for financial support via the MATOREN state-to-country program and Alain Lemaitre, Simon Dobosz, Miguel Pernes and François Gaudard for helpful technical assistance.

References

[1] Bailey C. A review of biocomposite development. JEC Compos Mag 2009;46:32–3.
[2] Bledzki AK, Gassan J. Composites reinforced with cellulose based fibres. Prog Polym Sci 1999;24:221–74.
[3] Mohanty AK, Misra M, Hinrichsen G. Biofibres, biodegradable polymers and biocomposites: an overview. Macromol Mater Eng 2000;276(277):1–24.
[4] Andersons J, Porike E, Sparnins E. Modeling strength scatter of elementary flax fibers: the effect of mechanical damage and geometrical characteristics. Composites: Part A 2011;42:543–9.
[5] Placet V, Trivaudey F, Cisse O, Gucheret-Retel V, Boubakar ML. Diameter dependence of the apparent tensile modulus of hemp fibres: a morphological, structural or ultrastructural effect? Composites: Part A 2012;43:275–87.
[6] Liu WJ, Drzal L, Mohanty T, Misra AK. Influence of processing methods and fiber length on physical properties of kenaf fiber reinforced soy based biocomposites. Composites: Part B 2007;38:352–9.
[7] Ausias G, Bourmaud A, Coroller G, Baley C. Study of the fibre morphology stability in polypropylene–flax composites. Polym Degrad Stabil 2013;98:1216–24.
[8] Chinga-Carrasco G, Solheim O, Lenes M, Larsen A. A method for estimating the fibre length in fibre-PLA composites. J Microsc 2013;250:15–20.
[9] Forgacs OL, Mason SG. Particle motions in sheared suspensions IX: spin and deformation of threadlike particles. J Colloid Sci 1959;14:457–72.
[10] Inceoglu F, Ville J, Ghamri N, Pradel JL, Durin A, Valette R, et al. Correlation between processing conditions and fibre breakage during compounding of glass fibre-reinforced polyamide. Polym Compos 2011;32:1842–50.
[11] Durin A, de Micheli P, Ville J, Inceoglu F, Valette R, Vergnes B. A matricial approach of fibre breakage in twin-screw extrusion of glass fibres reinforced thermoplastics. Composites: Part A 2013;48:47–56.
[12] Ville J, Inceoglu F, Ghamri N, Pradel JL, Durin A, Valette R, et al. Influence of extrusion conditions on fibre breakage along the screw profile during twin screw compounding of glass fibre-reinforced polyamide. Int Polym Proc 2013;28:49–57.
[13] Le Duc A, Vergnes B, Budtova T. Polypropylene/natural fibres composites: analysis of fibre dimensions after compounding and observations of fibre rupture by rheo-optics. Composites: Part A 2011;42:1727–37.
[14] Bourmaud A, Baley C. Effects of thermomechanical processing on the mechanical properties of biocomposite flax fibers evaluated by nanoindentation. Polym Degrad Stabil 2010;95:1488–94.
[15] Quijano-Solis C, Yan N, Zhang SY. Effect of mixing conditions and initial fiber morphology on fiber dimensions after processing. Composites: Part A 2009;40:351–8.
[16] Puglia D, Terenzi A, Barbosa SE, Kenny JM. Polypropylene–natural fibre composites. Analysis of fibre structure modification during compounding and its influence on the final properties. Compos Interface 2008;15:111–29.
[17] El-Sabbagh A, Steuernagel L, Ziegmann G. Effect of twin screw extruder layout on natural fibre polymer composites. In: SAMPE-Symposium, Institut für Kunststoffverarbeitung (IKV) an der RWTH, Aachen, 16–17 February, 2011.
[18] Bengtsson M, Le Baillif M, Oksman K. Extrusion and mechanical properties of highly filled cellulose fibre-polypropylene composites. Composites: Part A 2007;38:1922–31.
[19] Gamon G, Evon Ph, Rigal L. Twin-screw extrusion impact on natural fibre morphology and material properties in poly(lactic acid) based biocomposites. Indus Crops Prod 2013;46:173–85.
[20] Beaugrand J, Berzin F. Lignocellulosic fiber reinforced composites: influence of compounding conditions on defibrization and mechanical properties. J Appl Polym Sci 2013;128:1227–38.
[21] Jiang B, Liu C, Zhang C, Wang B, Wang Z. The effect of non-symmetric distribution of fiber orientation and aspect ratio on elastic properties of composites. Composites: Part B 2007;28:24–34.
[22] Vergnes B, Della Valle G, Delamare L. A global computer software for polymer flows in corotating twin screw extruders. Polym Eng Sci 1998;38:1781–92.

[23] Šimkovic I. Trends in thermal stability study of chemically modified lignocellulose materials. In: Leo B, editor. Polymer degradation and stability research developments. Albertov: Nova Science Publishers; 2007.
[24] Le Moigne N, van den Oever M, Budtova T. A statistical analysis of fibre size and shape distribution after compounding in composites reinforced by natural fibres. Composites: Part A 2011;42:1542–50.
[25] Legland D, Beaugrand J. Automated clustering of lignocellulosic fibres based on morphometric features and using clustering of variables. Indus Crops Prod 2013;45:253–61.
[26] Shon K, Liu D, White JL. Experimental studies and modelling of development of dispersion and fibre damage in continuous compounding. Int Polym Proc 2005;20:322–31.